myjournal manuscript No.
(will be inserted by the editor)

Hierarchical structures in Northern Hemispheric extratropical winter ocean-atmosphere interactions

Marc Wiedermann · Jonathan F. Donges · Dörthe Handorf · Jürgen Kurths · Reik V. Donner

Received: date / Accepted: date

Abstract In recent years extensive studies on the Earth's climate system have been carried out by means of advanced complex network statistics. The great majority of these studies, however, have been focusing on investigating interaction structures within single climatological fields directly on or parallel to the Earth's surface. In this work, we develop a novel approach of node weighted interacting network measures to study ocean-atmosphere coupling in the Northern Hemisphere and construct 18 coupled climate networks, each consisting of two subnetworks. In all cases, one subnetwork represents monthly sea-surface temperature (SST) anomalies while the other is based on the monthly geopotential height (HGT) of isobaric surfaces at different pressure levels covering the troposphere as well as the lower stratosphere. The weighted cross-degree density proves to be consistent with the leading coupled pattern obtained from maximum covariance analysis, while network measures of higher order allow for a further analysis of the correlation structure between the two fields. Zonally averaged local network measures reveal the sets of latitudinal bands for which there exists a strong coupling between parts of the ocean and the atmosphere. Global network measures quantify the strength of these interactions and identify atmospheric layers which form dynamical clusters of comparable strength with the ocean. All measures consistently indicate that the ocean-to-atmosphere coupling in the Northern Hemisphere follows a hierarchical structure in the sense that large areas in the ocean couple with multiple dynamically dissimilar areas in the atmosphere. We propose, that these patterns can be attributed to large-scale ocean currents that interact with and mediate between smaller dynamical clusters in the atmosphere.

Keywords coupled climate networks · ocean-atmosphere interaction · node-weighted network measures · hierarchical networks

Marc Wiedermann
Potsdam Institute for Climate Impact Research — P.O. Box 60 12 03, 14412 Potsdam, Germany
Department of Physics, Humboldt University — Newtonstr. 15, 12489 Berlin, Germany
E-mail: marc.wiedermann@pik-potsdam.de

Jonathan F. Donges
Potsdam Institute for Climate Impact Research — P.O. Box 60 12 03, 14412 Potsdam, Germany
Stockholm Resilience Centre, Stockholm University — Kräftriket 2B, 114 19 Stockholm, Sweden

Dörthe Handorf
Alfred Wegener Institute, Helmholtz Centre for Polar and Marine Research — Telegrafenberg A43, 14473 Potsdam, Germany

Jürgen Kurths
Potsdam Institute for Climate Impact Research — P.O. Box 60 12 03, 14412 Potsdam, Germany
Department of Physics, Humboldt University — Newtonstr. 15, 12489 Berlin, Germany
Institute for Complex Systems and Mathematical Biology, University of Aberdeen — Aberdeen AB24 3FX, United Kingdom
Department of Control Theory, Nizhny Novgorod State University — Gagarin Avenue 23, 606950 Nizhny Novgorod, Russia

Reik V. Donner
Potsdam Institute for Climate Impact Research — P.O. Box 60 12 03, 14412 Potsdam, Germany

1 Introduction

In the last years, complex network analysis has been established as a powerful tool to study statistical interdependencies in the climate system (Donges et al, 2009b; Tsonis and Roebber, 2004; Tsonis et al, 2008, 2006; Donges et al, 2015) Links in the so-called climate networks represent functional interdependencies indicated by significant correlation (Donges et al, 2009a,b; Radebach et al, 2013; Paluš et al, 2011) or the synchronous occurrence of extreme events (Stolbova et al, 2014; Boers et al, 2013; Malik et al, 2010, 2011; Boers et al, 2014b) in climatic time series taken at different grid points or measurement sites on or parallel to the Earth's surface. In addition to studies on observational data of climate dynamics, climate networks have also been applied successfully to hindcast extreme events, such as extreme precipitation in South America (Boers et al, 2014a), or to predict the occurrence of El Niño episodes (Ludescher et al, 2013, 2014). So far, most studies conducted within the framework of climate networks focused solely on the dynamics within a single climatological field or layer. Besides atmospheric characteristics like surface air temperature or precipitation, recent studies have also addressed ocean dynamics represented by ocean temperature variabilities at the surface (Feng and Dijkstra, 2014; Tantet and Dijkstra, 2014) or different depths (van der Mheen et al, 2013) as well as the spatio-temporal variability in the strength of the Atlantic meridional overturning circulation (Feng et al, 2014).

It is well known, however, that the dynamics within the two major subcomponents of the Earth's climate system, ocean and atmosphere, are closely entangled (Trenberth and Hurrell, 1994; Frankignoul et al, 2001). Examples for these interrelationships include the North Atlantic eddy-driven jet stream (Woollings et al, 2010) or the Pacific ocean forcing to the atmosphere which is closely related to the dynamics of the El Niño Southern Oscillation (Wyrtki, 1975). In addition, there is evidence for strong ocean-atmosphere feedbacks induced by major oceanic currents in the North Atlantic as well as the North Pacific (Kwon et al, 2010; Nonaka and Xie, 2003). The study of a single climatological field, however, is not sufficient to fully disentangle and understand emerging dynamics in either of the two coupled subsystems, ocean and atmosphere.

Inspired by approaches to investigate the interaction structure between different subsystems such as infrastructure networks (Vespignani, 2010; Buldyrev et al, 2010; Boccaletti et al, 2014) a novel set of interacting network measures has been proposed by Donges et al (2011) which provides a general tool to quantify interdependencies between subcomponents in complex coupled climate networks. The latter framework has been successfully applied to investigate the interactions between different layers of geopotential height fields, where each isobaric surface forms a subcomponent of a larger climate network.

In order to also include ocean dynamics into the analysis, we follow the approach by Donges et al (2011) and present an exploratory study to understand and quantify ocean-atmosphere interactions in the Northern Hemisphere mid-to-high latitudes during winter at monthly scales. We construct in total 18 coupled climate networks consisting of two layers each, one layer representing sea surface temperature (SST) anomalies and the other geopotential height fields (HGT) at different pressure levels from 1000 to 10 mbar covering the entire troposphere as well as the lower stratosphere.

Our area of study covers the whole Northern Hemisphere north of 30°N so that the density of grid points in the considered climate data sets increases rapidly towards the poles and induces biases in the unweighted network measures (Tsonis et al, 2006; Radebach et al, 2013). Therefore, the standard interacting network approach by Donges et al (2011) is not sufficient in the present case. To overcome the problem associated with heterogeneous spatial density of grid points interpreted as nodes of the climate network, Heitzig et al (2012) introduced a novel set of network measures that takes into account the different sizes or weights of nodes in the network. By following an axiomatic approach, each *standard* (or unweighted) network measure can be transformed into its weighted counterpart, the so-called *node splitting invariant* (n.s.i.) network measure. Corresponding n.s.i. measures have also been derived by Zemp et al (2014) for edge-weighted and directed networks.

To quantify the topology of coupled climate networks, we rely in this work on the previously defined versions of local (i.e. node-wise) n.s.i. interacting network measures (Feng et al, 2012; Wiedermann et al, 2013) and additionally derive further weighted global network measures following the approach introduced by Heitzig et al (2012). This allows us to assess and compare the macroscopic interaction structure in each of the 18 coupled climate networks.

Additionally, we compare the results of a maximum covariance analysis (MCA) (e.g. von Storch and Zwiers, 2001), a well-established standard tool from statistical climatology, with the cross-degree density of nodes in the different subnetworks and confirm expected similarities between the two measures (Donges et al, 2015). By utilizing network measures of higher order such as the n.s.i. local cross-clustering coefficient, we find that the ocean-to-atmosphere coupling exhibits a hierarchical structure, in which individual parts or areas of the ocean surface interact with multiple dynamically dissimilar parts of the atmosphere.

In general, our method serves to improve the understanding and quantification of mid-to high latitude coupling between atmosphere and ocean at monthly time scales and complements the information obtained from classical statistical methods, such as MCA.

The remainder of this paper is organized as follows. Section 2 introduces the data sets and all methods, i.e. maximum covariance analysis and climate network analysis, that are applied in this study. Section 3 presents all results of the analysis followed by conclusions and an outlook discussing future research tasks in Section 4.

2 Data & Methods

2.1 Data description

We construct coupled climate networks from two different climatological observables in order to investigate their interaction structure. One subnetwork is based on monthly anomalies of geopotential height (HGT) fields obtained from the ERA40 reanalysis project of the European Centre for Medium-Range Weather Forecast (Uppala et al, 2005). The data is given on a regular latitude/longitude grid with a spatial resolution of $\Delta\lambda = \Delta\phi = 2.5°$. In total, we investigate 18 layers of HGT fields. The corresponding pressure at each isobaric surface as well as the average geopotential height are given in Tab. 1. The second subnetwork is constructed from the monthly averaged SST field (HadISST1) provided by the Met Office Hadley Centre (Rayner et al, 2003) with a resolution of $\Delta\lambda = \Delta\phi = 1°$. All grid points with corresponding time series containing missing values are removed from the data set as they represent areas which are at least temporarily covered by sea-ice.

For our analysis we investigate all grid points north of $\lambda = 30°$N excluding those directly located at the North Pole. Both data sets are cropped in their temporal extent to cover the same time span from January 1958 to December 2001 and, hence, each time series consists of $T = 528$ temporal sampling points. We obtain a total number of $N_s = 6201$ grid points for the SST data and $N_i = 3456$ grid points for each isobaric surface i of HGT. For both data sets, we remove the annual cycle by subtracting the climatological mean for each month from each time series. Since our focus is set on the interaction structure between ocean and atmosphere during winter months (DJF), we use only the corresponding values which yields a length of each time series of $\tau = 132$ data points.

Table 1 Air pressure p_i and associated mean geopotential height Z_i for each isobaric surface i.

Layer i	Air pressure p_i [mbar]	Geopotential height Z_i [km]
0	10	30.9
1	20	26.3
2	30	23.7
3	50	20.5
4	70	18.4
5	100	16.2
6	150	13.7
7	200	11.8
8	250	10.4
9	300	9.2
10	400	7.2
11	500	5.6
12	600	4.2
13	700	3.0
14	775	2.2
15	850	1.4
16	925	0.8
17	1000	0.1

2.2 Maximum covariance analysis (MCA)

Consider two sets of time series $\{X_{s_n}(t)\}_{n=1}^{N_s}$ and $\{X_{i_m}(t)\}_{m=1}^{N_i}$ representing two different climatological fields, which in the scope of our application are the SST field (in what follows indicated by the index s) and one layer i of HGT (see also Tab. 1). Further assume the individual time series in both fields to be normalized to zero mean and unit variance. The linear lag-zero cross-covariance matrix $\mathbf{C}_{si}$ with entries $C_{s_n i_m}$ is then defined as

$$C_{s_n i_m} = \frac{1}{\tau} \sum_{t=1}^{\tau} X_{s_n}(t) X_{i_m}(t), \tag{1}$$

where $n = 1, \ldots, N_s$, $m = 1, \ldots, N_i$ and τ denotes the total number of temporal sampling points in the two time series. Due to the heterogeneous spatial distribution of grid points in the present data sets all matrix entries $C_{s_n i_m}$ are additionally multiplied by the square roots of the cosine of latitudinal positions $\lambda_\bullet$ to ensure equal weighting. This then yields the weighted cross-covariance matrix $\mathbf{C}^w_{si}$ with entries

$$C^w_{s_n i_m} = \sqrt{\cos\lambda_{s_n} \cos\lambda_{i_m}} C_{s_n i_m}. \tag{2}$$

Analogously to empirical orthogonal function (EOF) analysis (e.g. Ghil et al, 2002; Hannachi et al, 2007), MCA identifies orthonormal pairs of coupled patterns $\mathbf{p}_s^{(m)} = (p_{s_1}^{(m)} \ldots p_{s_{N_s}}^{(m)})$ and $\mathbf{p}_i^{(m)} = (p_{i_1}^{(m)} \ldots p_{i_{N_i}}^{(m)})$ for $m = 1, \ldots, R$ (with R being the rank of $\mathbf{C}_{si}$) which explain as much as possible of the covariance between pairs of time series taken from the two different climatological fields (e.g. Bretherton et al, 1992; von Storch and Zwiers, 2001). The coupled patterns are obtained

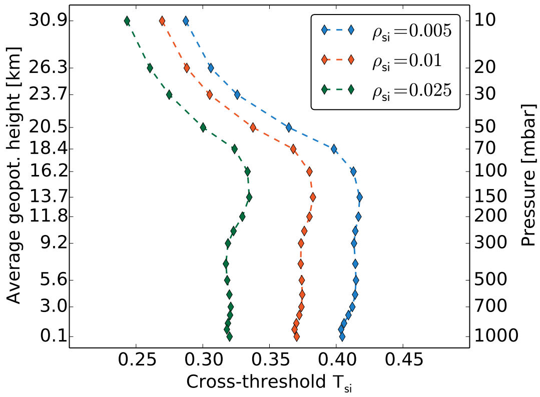

Fig. 1 Cross-threshold T_{si} between the subnetwork constructed from the SST field and all 18 isobaric surfaces of HGT in winter for different standard (unweighted) cross-link densities.

by solving the eigenvalue problem of the weighted cross-covariance matrix,

$$\mathbf{C}_{si}^{w}\mathbf{p}_i^{(m)} = \sigma_m \mathbf{p}_s^{(m)}, \quad (3)$$

$$(\mathbf{C}_{is}^{w})^{\mathbf{T}}\mathbf{p}_s^{(m)} = \sigma_m \mathbf{p}_i^{(m)}. \quad (4)$$

They are ordered by according to their respective singular values σ_k with $\sigma_1 \geq \sigma_2 \geq \ldots \geq \sigma_R$. Hence, σ_1 denotes the largest of the set of R singular values that can be found to solve the above equations. Therefore, $\mathbf{p}_i^{(1)}$ and $\mathbf{p}_s^{(1)}$ are referred to as the *leading* coupled patterns representing the largest fraction of squared covariance between the two climatological fields given by σ_1^2.

2.3 Coupled climate network construction

In climate networks, each node represents a climatological time series and links indicate significant similarity between two series. Hence, the $N \times N$ ($N = N_s + N_i$) similarity matrix gives the pairwise statistical relationships between all time series considered for the network construction. Here, we independently construct coupled climate networks for all combinations of the SST field and each of the 18 isobaric surfaces of HGT, which shall be investigated separately and rely on the linear Pearson correlation coefficient as an appropriate measure of dynamical similarity. Hence, the correlation matrix has the form

$$\mathbf{C} = \begin{pmatrix} \mathbf{C}_{ss} & \mathbf{C}_{si} \\ \mathbf{C}_{is} & \mathbf{C}_{ii} \end{pmatrix}. \quad (5)$$

The two block matrices $\mathbf{C}_{ss}$ ($N_s \times N_s$) and $\mathbf{C}_{ii}$ ($N_i \times N_i$) represent the (internal) correlation matrices of the SST and HGT fields, respectively, which consist of elements

$$C_{s_n s_m} = \frac{1}{\tau}\sum_{t=1}^{\tau} X_{s_n}(t) X_{s_m}(t), \quad n, m = 1, \ldots, N_s, \quad (6)$$

$$C_{i_n i_m} = \frac{1}{\tau}\sum_{t=1}^{\tau} X_{i_n}(t) X_{i_m}(t), \quad n, m = 1, \ldots, N_i. \quad (7)$$

The elements of $\mathbf{C}_{si} = \mathbf{C}_{is}^{\mathbf{T}}$ are derived according to Eq. (1). Note, that for the network construction (in contrast to the computation of the leading coupled patterns) we construct the coupled climate networks from the *unweighted* correlation matrix $\mathbf{C}$, while the correction for the heterogeneous spatial distribution of nodes is implemented into the corresponding network measures (see Sec. 2.4).

From the correlation matrix $\mathbf{C}$ one generally derives the network's adjacency matrix $\mathbf{A}^+$ by setting a fixed threshold T such that only a certain fraction (i.e. the link density ρ) of strongest correlations is represented by links in the resulting climate network. For obtaining the adjacency matrix $\mathbf{A}^+$ of coupled climate networks, we refine this procedure by fixing a desired link density $\rho_s = \rho_i = 0.01$ for the structure of internal links within the two subnetworks representing SST and HGT fields, respectively. This means that only nodes with a correlation above the empirical 99th percentile of correlations between all time series within each field are connected. This condition then leads to internal correlation thresholds T_s for the SST field and T_i for each isobaric surface of GPH. Usually, the dynamics within the different climatological fields shows much higher cross-correlations than the dynamics between them. We account for this fact by assuming the fraction of significant interactions between the climatological fields to be lower than those within them. Specifically, we request a cross-link density of $\rho_{si} = 0.005 < \rho_s = \rho_i$, which is lower than the internal ones, and derive a cross-threshold T_{si} for each layer of HGT individually (Fig. 1). The different values of T_{si} already give an impression of the interaction strenghts between the SST field and the different isobaric layers: low thresholds generally indicate weaker interactions while high thresholds imply strong correlation between both different fields.

Using the different thresholds introduced above, we obtain the coupled climate network's adjacency matrix by individually thresholding the absolute correlation values between and within both fields as

$$\mathbf{A}^+ = \begin{pmatrix} \Theta(|\mathbf{C}_{ss}| - T_s) & \Theta(|\mathbf{C}_{si}| - T_{si}) \\ \Theta(|\mathbf{C}_{is}| - T_{si}) & \Theta(|\mathbf{C}_{ii}| - T_i) \end{pmatrix},$$

where $\Theta(\cdot)$ denotes the Heaviside function. Note that in most recent studies on climate networks self-loops (resulting in a non-vanishing trace of the adjacency matrix) have been excluded. In this case the adjacency matrix is usually denoted as $\mathbf{A}$. Since we aim to apply node splitting invariant network measures (see below) to quantify the network's topology we specifically demand each node to be connected with itself. The resulting matrix $\mathbf{A}^+$ is referred to as the *extended* adjacency matrix (Heitzig et al, 2012).

2.4 Interacting network characteristics

The local (point-wise) and global structure of a climate network can be quantified by a variety of network measures (Newman, 2003; Albert and Barabási, 2002; Donges et al, 2009b), which generally can be interpreted as specific operations on the adjacency matrix. The climate networks in this study are constructed from climate data sets where the density of grid points and, hence, the density of nodes in the network, rapidly increases towards the North pole. In order to avoid bias in the evaluation of the climate network's structure, we account for this effect by relying on node weighted network measures and value nodes with a gradually decreasing weight as one moves from the equator to the pole. To quantify the ocean-atmosphere interactions at each node we focus on two previously defined node weighted local network measures, the n.s.i cross-degree (Feng et al, 2012) and the n.s.i. local cross-clustering coefficient (Wiedermann et al, 2013). In addition, we utilize the construction mechanism introduced by Heitzig et al (2012) to convert global interacting network measures (Donges et al, 2011) into their weighted counterparts.

2.4.1 Preliminaries

Consider a coupled climate network $G = (V, E)$ with a set of nodes V, links E and the number of nodes $N = |V|$. Identifying every node $v \in V$ with a natural number $p = 1, \ldots, N$, the network G is represented by its adjacency matrix $\mathbf{A}$ with $A_{pq} = 1$ if $(p, q) \in E$, $A_{pq} = 0$ if $(p, q) \notin E$. In this study, the network is composed of two subnetworks, $G_s = (V_s, E_{ss})$ representing the ocean and $G_i = (V_i, E_{ii})$ representing the atmosphere. The set of nodes V decomposes into subsets V_s and V_i such that each node belongs to exactly one subnetwork (i.e., $V = V_s \cup V_i$ and $V_s \cap V_i = \emptyset$). Likewise, the set of links E then splits into internal link sets E_{ss} and E_{ii} connecting nodes within a subnetwork and cross-link sets E_{si} connecting nodes $v \in V_s$ with nodes $q \in V_i$ in the subnetworks G_s and G_i, respectively (Donges et al, 2011).

In the present case (as for all regular gridded climate data sets) the share on the entire area of the surface that is represented by each node is governed by its latitudinal position λ_v on the grid. Following Tsonis et al (2006), we therefore assign to each node v in the climate network a weight

$$w_v = \cos \lambda_v. \tag{8}$$

Heitzig et al (2012) introduced a novel set of *node splitting invariant* (n.s.i.) network measures to quantify the topology of a climate network with such a heterogeneous spatial node density for the case of a single-layer network and, hence, only one climate variable under study. In fact, the n.s.i. network measures are not restricted to climate networks but can be utilized to study any type of single-layer complex network where nodes represent entities of different weights. Heitzig et al (2012) further showed that each complex network measure can be transformed into its weighted counterpart by using a four-step construction mechanism:

(a) Sum up weights w_v whenever the unweighted measure counts nodes.
(b) Treat every node $v \in V$ as connected with itself.
(c) Allow equality for v and q wherever the original measure involves a sum over distinct nodes v and q.
(d) "Plug in" n.s.i. versions of measures wherever they are used in the definition of other measures.

From the definition of the adjacency matrix $\mathbf{A}^+$ in Eq. (8) we note that step (b) of the above scheme is in our case already fulfilled. Wiedermann et al (2013) and Zemp et al (2014) recently utilized the proposed scheme to convert local interacting network measures as well as measures for directed networks into their weighted counterparts. Here, we additionally derive n.s.i. versions of some global cross-network measures that were introduced by Donges et al (2011).

2.4.2 Local measures

For quantifying local cross-network interactions in coupled climate networks we rely on two measures, n.s.i. cross-degree k_v^{j*} and n.s.i. local cross-clustering coefficient $\mathcal{C}_v^{j*}$, that were introduced by Wiedermann et al (2013) and (for the case of the n.s.i. cross-degree) by Feng et al (2012). These two measures are defined as

$$k_v^{j*} = \sum_{q \in V_j} w_q A_{vq}^+, \tag{9}$$

$$\mathcal{C}_v^{j*} = \frac{1}{\left(k_v^{j*}\right)^2} \sum_{p,q \in V_j} A_{vp}^+ A_{pq}^+ A_{qv}^+ w_q w_p \in [0, 1]. \tag{10}$$

In contrast to the unweighted cross-degree

$$k_v^j = \sum_{q \in V_j} A_{vq}^+ \tag{11}$$

which simply counts nodes $q \in V_j$ that are connected with $v \in V_i$, k_v^{j*} is proportional to the share on the considered overall ice-free ocean or isobaric surface area, respectively, that is connected with nodes $v \in V_j$ in the other subnetwork. It therefore gives a notion of how similar the dynamics at a node $v \in V_i$ is to that of the other climate variable observed at all available grid points.

Similar to k_v^{j*}, $\mathcal{C}_v^{j*}$ no longer relies on the counting of distinct triangles in the network (as for the classical local clustering coefficient (Newman, 2003)) but on the weighted sum of occurrences of triples of connected areas within the two subnetworks. It gives the probability that an area represented by a node $v \in V_i$ is connected with two mutually connected, hence, dynamically similar, areas in the opposite subnetwork. In this spirit $\mathcal{C}_v^{j*}$ estimates how likely areas in the coupled system are to form clusters of dynamical equivalence between the different climatological fields, or subsystems under study. Hence, we interpret a high local cross-clustering coefficient as representing confined regions of similar dynamics at different nodes or measurement sites and, hence, a strong coupling between them.

In order to make the n.s.i. cross-degree k_v^{j*} comparable between the two subnetworks, we normalize it by the maximum possible weight that nodes $v \in V_i$ can be connected with,

$$\kappa_v^{j*} = \frac{\sum_{q \in V_j} w_q A_{vq}^+}{W_j} \in [0,1]. \tag{12}$$

In the spirit of earlier work by Donges et al (2012) and Donner et al (2010), we refer to this quantity as the *n.s.i. cross-degree density*. Here, $W_j = \sum_{q \in V_j} w_q$ denotes the total weight of nodes $q \in V_j$. For the case of a single-layer network, a measure similar to the n.s.i. cross-degree density has been introduced by Tsonis et al (2006) in terms of the *area weighted connectivity* which measures the share on the subdomain of interest represented by the entire network G that is connected with any nodes $v \in V$.

Generally, Wiedermann et al (2013) and Zemp et al (2014) showed that the weighted local cross-network measures improve the representation of a network's topology with inhomogeneous node density within the domain of interest in comparison with its unweighted counterparts.

Donges et al (2015) showed that for the unweighted case cross-degree and leading coupled patterns display high similarity if the first coupled patterns explain a high fraction of the system's covariance. A similar assessment can be made for the similarity between the leading coupled patterns obtained from a weighted cross-covariance matrix and the n.s.i. cross-degree (see Appendix A).

2.4.3 Global measures

In addition to local (per node) network measures we also aim to characterize the macroscopic interaction structure of each pair of coupled climate networks by means of global network properties. For coupled climate networks a variety of unweighted measures have been proposed by Donges et al (2011). Here, we utilize the construction mechanism by Heitzig et al (2012) to convert a selection of them into their weighted counterparts as well.

N.s.i. cross-link density The (unweighted) cross-link density ρ_{ij} measures the share of links present between two different subnetworks with respect to the number of possible links. When constructing climate networks, this quantity is usually kept fixed and utilized to obtain the cross-threshold T_{ij} above which correlations between time series at the corresponding grid points are considered significant and the respective nodes v_i and v_j are treated as linked. The cross-link density ρ_{ij} is commonly defined as the average normalized cross-degree (Donges et al, 2011),

$$\begin{aligned}\rho_{ij} &= \frac{\sum_{p \in V_i} \sum_{q \in V_j} A_{pq}}{N_i N_j} \\ &= \frac{\sum_{v \in V_i} k_v^j}{N_i N_j} = \frac{\sum_{v \in V_j} k_v^i}{N_i N_j}\end{aligned} \tag{13}$$

with N_i and N_j being the number of nodes in the two subnetworks. Analogously, the weighted average of the n.s.i. cross-degree density yields the n.s.i. cross-link density

$$\rho_{ij}^* = \frac{\sum_{v \in V_j} w_v \kappa_v^{j*}}{W_i} = \frac{\sum_{v \in V_i} w_v \kappa_v^{i*}}{W_j}, \tag{14}$$

which measures the average share of the Earth's surface that nodes in either of the two subnetworks are connected with. Hence, high values of ρ_{ij}^* indicate a strong similarity between the two climate variables under study.

N.s.i. global cross-clustering coefficient. The global cross-clustering coefficient $\mathcal{C}_{ij}$ of a subnetwork G_i gives the probability that for a randomly chosen node $v \in V_i$ one finds neighbors $p, q \in V_j$ that are mutually linked. It is defined as the arithmetic mean over all local cross-clustering coefficients $\mathcal{C}_v^j$,

$$\mathcal{C}_{ij} = \frac{1}{N_i} \sum_{v \in V_i} \mathcal{C}_v^j. \tag{15}$$

This measure can be converted into its n.s.i. counterpart by calculating the weighted mean over all values of $\mathcal{C}_v^{j*}$,

$$\mathcal{C}_{ij}^* = \frac{1}{W_i} \sum_{v \in V_i} w_v \mathcal{C}_v^{j*}. \tag{16}$$

Again, analogously to the interpretation of the local n.s.i. measures, $\mathcal{C}_{ij}^*$ no longer only measures pure node-wise triangular structures but takes into account the share on the Earth's surface areas involved in the formation of triangular structures. Generally, high values of $\mathcal{C}_{ij}^*$ (which are induced by a dominance of connected triples between the two subnetworks under consideration) indicate strong transitivity in the underlying correlation structure.

N.s.i. cross-transitivity. The cross-transitivity $\mathcal{T}_{ij}$ gives the probability that two randomly drawn nodes $p, q \in V_j$ are connected if they have a common neighbor $v \in V_i$. It is given as

$$\mathcal{T}_{ij} = \frac{\sum_{v \in V_i} \sum_{p \neq q \in V_j} A_{vp} A_{pq} A_{qv}}{\sum_{v \in V_i} \sum_{p \neq q \in V_j} A_{vp} A_{qv}}. \tag{17}$$

Like $\mathcal{C}_{ij}$, the cross-transitivity is a measure of organization with respect to the interaction structure in a coupled network (Donges et al, 2011). However, in contrast to $\mathcal{C}_{ij}$, $\mathcal{T}_{ij}$ takes into account the increasing influence of nodes with high cross-degree and weighs them more heavily than nodes with low cross-degree. The node-weighted variant of $\mathcal{T}_{ij}$ can be written as

$$\begin{aligned}\mathcal{T}_{ij}^* &= \frac{\sum_{v \in V_i} \sum_{p,q \in V_j} w_v A_{vp}^+ w_p A_{pq}^+ w_q A_{qv}^+}{\sum_{v \in V_i} \sum_{p,q \in V_j} w_v A_{vp}^+ w_p w_q A_{qv}^+} \\ &= \frac{\sum_{v \in V_i} w_v (k_v^{j*})^2 \mathcal{C}_v^{j*}}{\sum_{v \in V_i} w_v (k_v^{j*})^2}.\end{aligned} \tag{18}$$

We note that both $\mathcal{C}_{ij}^*$ and $\mathcal{T}_{ij}^*$ similarly evaluate the transitivity of correlation between the two climatological variables under study and, hence, quantify a similar network property. They are derived, however, in a disjoint manner. One measure, $\mathcal{C}_{ij}^*$ is computed as the weighted average taken over $\mathcal{C}_v^{j*}$. In contrast, despite suggestions by Radebach et al (2013) to decompose the global transitivity into local contributions, the n.s.i. cross-transitivity $\mathcal{T}_{ij}^*$ is defined solely as a global network measure with no direct local counterpart. It is important to note that, in contrast to the n.s.i. cross-link density, n.s.i. cross-transitivity and n.s.i. global cross-clustering coefficient can be asymmetric in the sense that $\mathcal{T}_{ij}^* \neq \mathcal{T}_{ji}^*$ and $\mathcal{C}_{ij}^* \neq \mathcal{C}_{ji}^*$.

3 Results

3.1 Maximum covariance analysis (MCA)

We start our analysis by computing the leading coupled patterns between the SST field and the 18 HGT layers for winter months (DJF). Figure 2 displays the results for three representative layers of HGT at 50 mbar, 100 mbar and 500 mbar.

By applying MCA, we detect coherent large-scale patterns of winter SST, which co-vary with the winter atmospheric circulation structures instantaneously. The leading MCA patterns explain rather large amounts of 42%, 63% and 70% (for the 500, 100 and 50 mbar pressure level, respectively) of the squared covariance. At all levels, the leading MCA mode displays significant SST anomalies over the North Pacific with maximum values along the sub-Arctic front near 40°N, and anomalies of the opposite sign along the western coast of North America (Fig. 2A,C,E) (Frankignoul and Senchael, 2007; An and Wang, 2005). Over the North Atlantic, a dipole structure is seen between the northern part of the Gulf Stream and the Atlantic Ocean south of Greenland including parts of the Davis Strait and the North Atlantic current. This pattern resembles the first SST EOF for the Northern Hemisphere during winter (not shown).

This general SST pattern is co-varying with a pressure anomaly pattern showing a hemispheric annular-like structure in the upper troposphere and lower stratosphere (Fig. 2B,D). In the mid-troposphere (Fig. 2F), this pattern displays wave-like deviations from the annular structure, which show distinct similarities with the wave-train structure of the Pacific North American (PNA) pattern over the Pacific-North American sector. Therefore, the leading MCA mode relates negative SST anomalies along the sub-Arctic front to a positive PNA phase.

The second MCA mode (not shown, explaining 13%, 17% and 21% of the squared covariance fraction for the 500, 100 and 50 mbar pressure level, respectively) displays the strongest SST anomalies over the North Atlantic. Over that region, the SST pattern resembles the northern part of the North Atlantic SST tripole pattern which is related to the North Atlantic Oscillation (NAO) (e.g. Czaja and Frankignoul, 1999, 2002; Gastineau and Frankignoul, 2014). Accordingly, the co-varying atmospheric pattern in the middle troposphere shows the cold ocean/warm land (COWL) pattern (introduced by Wallace et al (1996)) including a NAO-like dipole over the North Atlantic. At higher levels, the co-varying atmospheric patterns display a pronounced wavenumber-2 pattern.

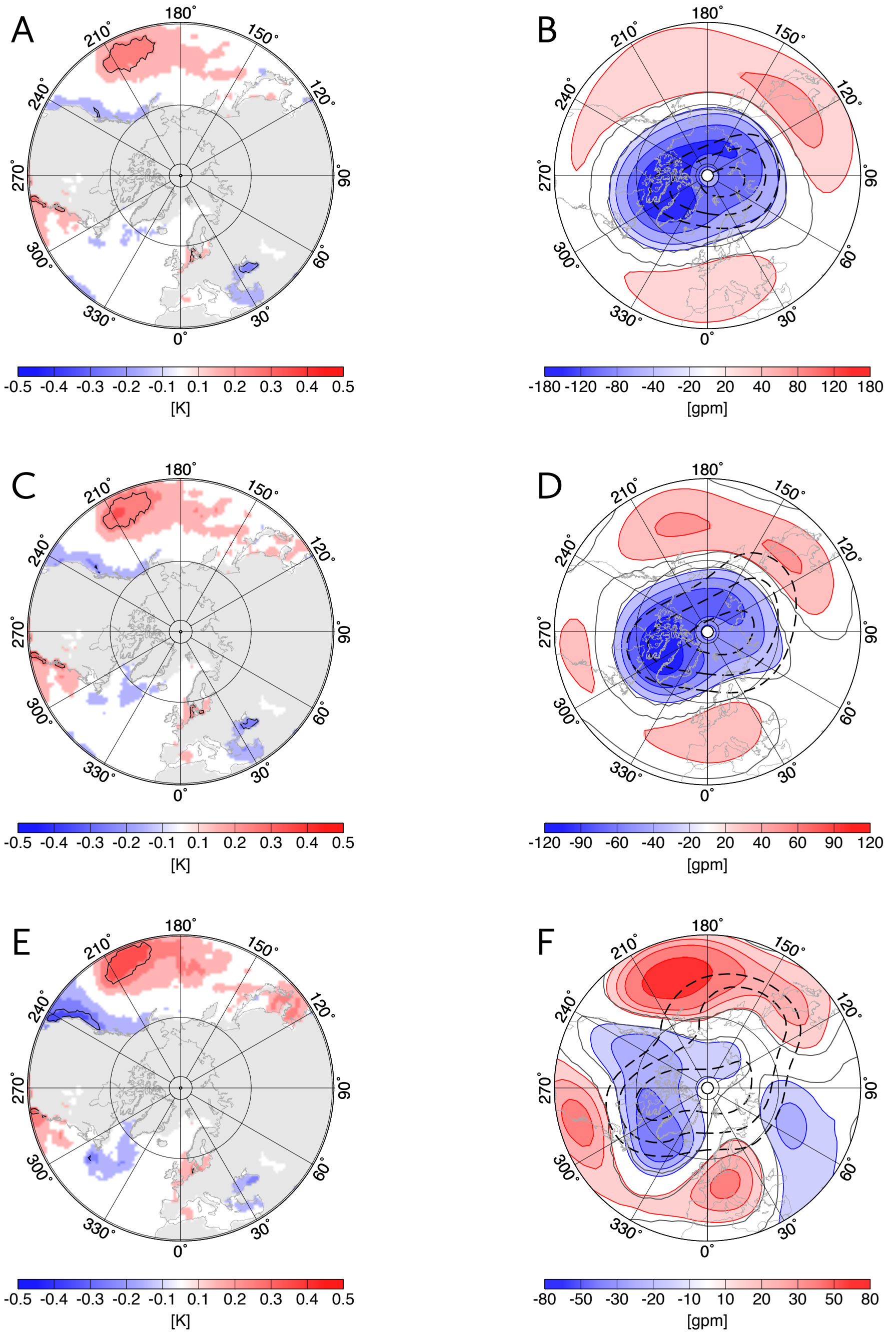

Fig. 2 Leading coupled patterns obtained from MCA between the SST field and three layers of geopotential height at 50 mbar (A and B), 100 mbar (C and D) and 500 mbar (E and F) in winter (DJF). The left column (A, C and E) displays the component in the SST and the right column (B, D and F) that in the respective HGT field.

By applying lagged MCA between SST and mid-tropospheric circulation fields, several studies for the North Atlantic and the North Pacific have shown that the squared covariance fraction is strongest and most significant at lags 0 and 1 month during late fall and winter (e.g. Czaja and Frankignoul, 1999; Wen et al, 2005; Liu et al, 2006; Frankignoul and Sennchael, 2007; Gastineau and Frankignoul, 2014). This points to the forcing of the SST by the dominant atmospheric pattern, which is the PNA pattern over the Pacific-North American sector (e.g. Frankignoul and Sennchael, 2007) and the NAO over the North Atlantic-European region (Czaja and Frankignoul, 1999; Gastineau and Frankignoul, 2014). On the other hand, results of lagged MCA analyses with the ocean leading by 1 to 4 months in Frankignoul and Sennchael (2007) and Gastineau and Frankignoul (2014) suggest that the SST anomalies have

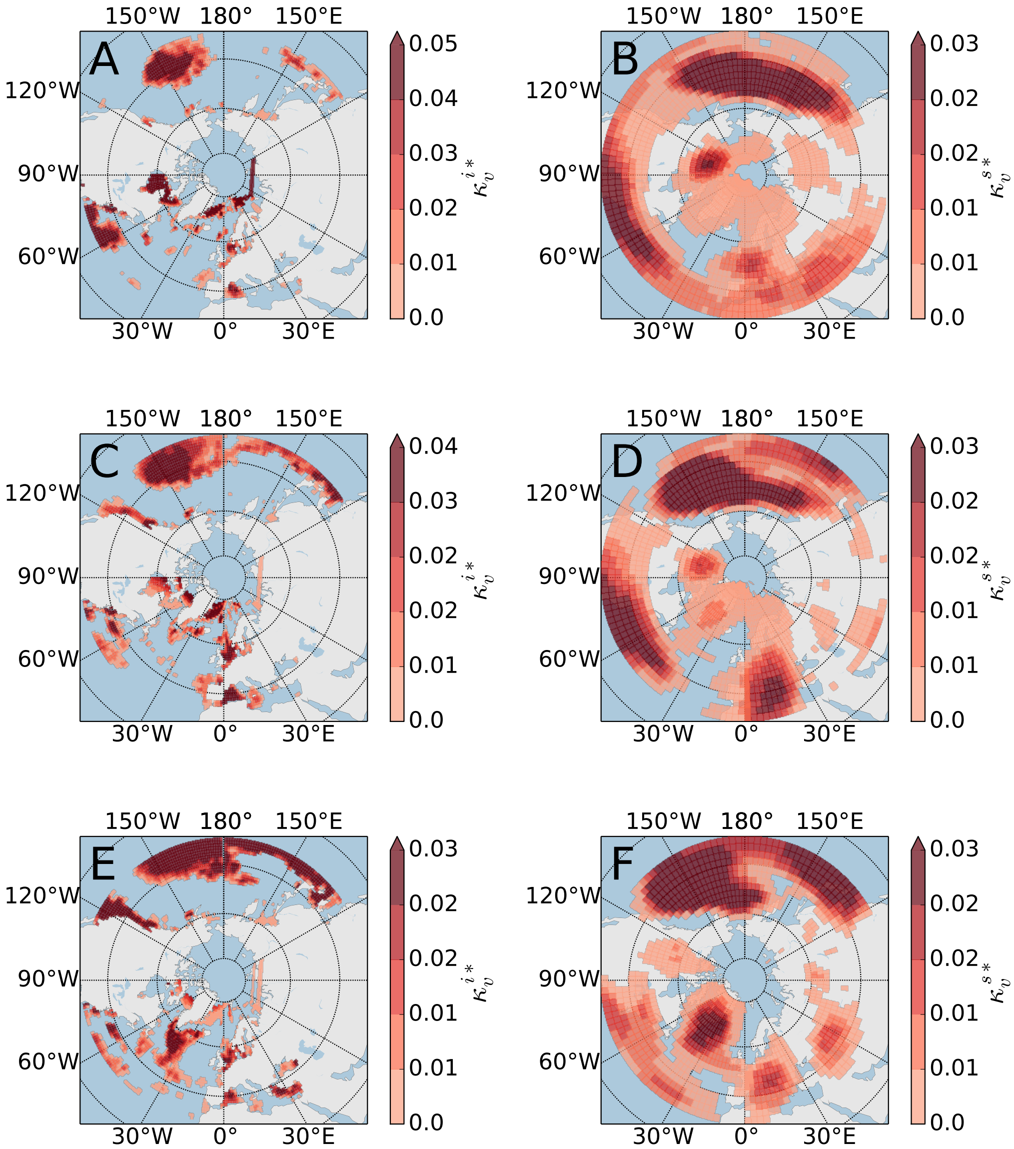

Fig. 3 N.s.i. cross-degree density for coupled climate networks constructed from the SST field and three layers of geopotential height at 50 mbar (A and B), 100 mbar (C and D) and 500 mbar (E and F) for winter months (DJF). The left column (A, C and E) displays the n.s.i. cross degree density κ_v^{i*} for links pointing from the SST into the HGT subnetwork while the right column (B, D and F) displays the n.s.i. cross-degree density κ_v^{s*} for links pointing from the HGT into the SST subnetwork. Only nodes with $\kappa_v^{i*} > 0$ and $\kappa_v^{s*} > 0$ are shown.

a substantial influence on the large-scale atmospheric circulation on these time-scales.

3.2 Local interacting network measures

In order to demonstrate the additional value of the coupled climate network analysis approach in comparison with MCA, we next study coupled climate networks between the SST field and the three previously considered layers of geopotential height (500 mbar, 100 mbar, 50 mbar). The n.s.i. cross-degree densities κ_v^{i*} and κ_v^{s*} are expected to display similar spatial structures as the corresponding leading coupled patterns (Donges et al, 2015) as the latter explains a high share of the cross-covariance between both fields (see Appendix).

As demonstrated in Fig. 3, the results for κ_v^{s*} and κ_v^{i*} indeed match well the results obtained from the MCA when comparing the locations of maximum values in the network's n.s.i. cross-degree density to those of maximum or minimum values in the leading mode of

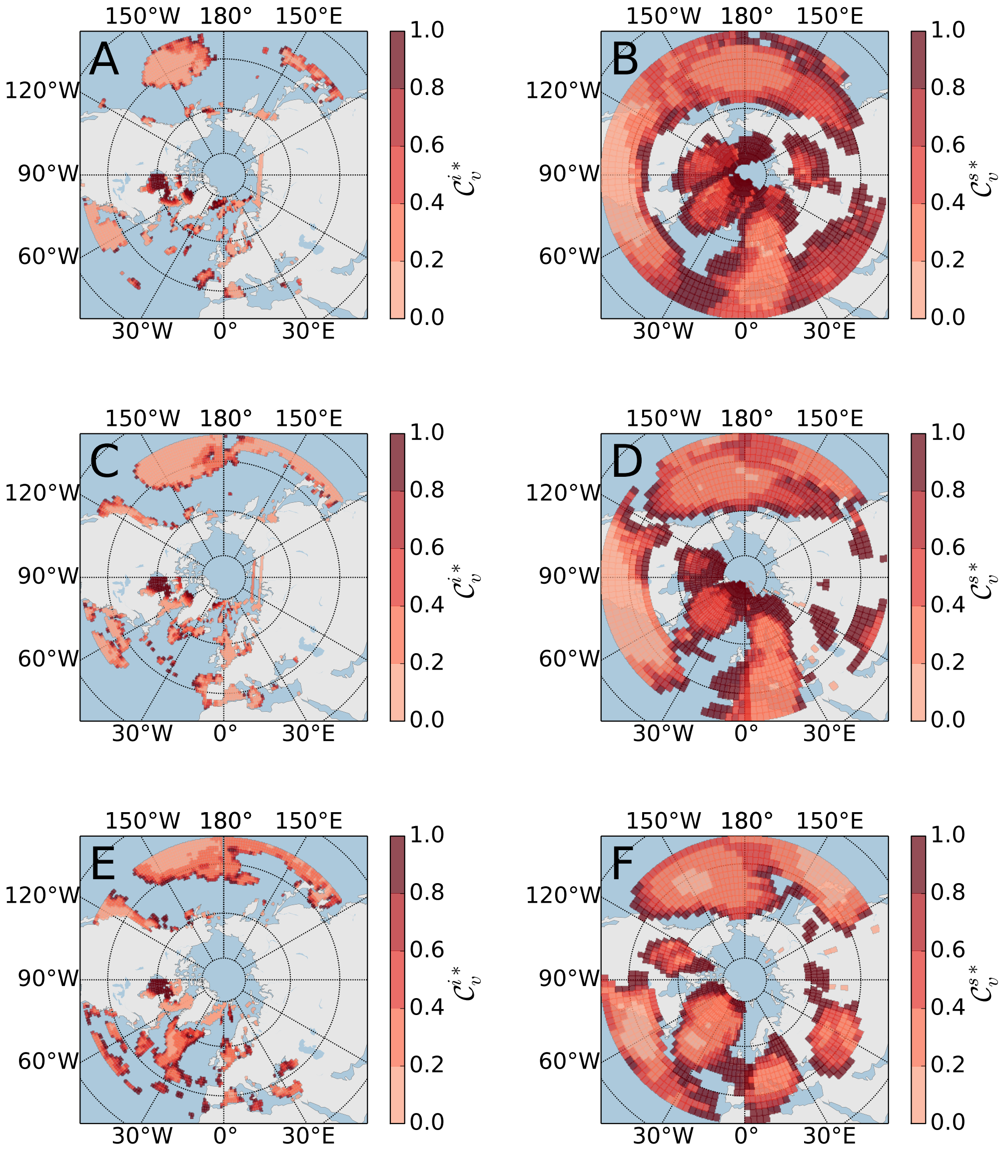

Fig. 4 As in Fig. 3 for the n.s.i. local cross-clustering coefficients $\mathcal{C}_v^{i*}$ and $\mathcal{C}_v^{s*}$.

the MCA. Note, that the n.s.i. cross-degree densities κ_v^{s*} and κ_v^{i*} take, per definition, only positive values, while coupled patterns display positive and negative values. Hence, κ_v^{s*} and κ_v^{s*} only reproduce structures that coincide with the absolute values of the leading coupled patterns.

Network analysis, however, now allows us to undertake a further in-depth analysis of the correlation structure between the different layers. The n.s.i. local cross-clustering coefficients $\mathcal{C}_v^{i*}$ and $\mathcal{C}_v^{s*}$ (Eq. (10)) give the probabilities, that the dynamics at a grid point in, e.g., the SST field is similar with that at two grid points in the HGT field, which themselves are dynamically similar.

Figure 4 presents the results for the n.s.i. local cross-clustering coefficients $\mathcal{C}_v^{i*}$ computed for all nodes in the SST field (Fig. 4A,C,E) and $\mathcal{C}_v^{s*}$ computed for all nodes in the HGT field (Fig. 4B,D,F). We find that for the SST field most nodes tend to display a low n.s.i. local cross-clustering coefficient $\mathcal{C}_v^{i*} < 0.2$ (Fig. 4A,C,E). Thus, these nodes preferentially couple with nodes in the HGT fields that themselves are dynamically dissimilar and, hence, unconnected (Fig. 5). In contrast, we find many nodes in the HGT fields which tend to show a comparatively high or intermediate n.s.i. local cross-clustering coefficient $0.4 < \mathcal{C}_v^{s*} < 1$ (Fig. 4B,D,F). Thus, in contrast to the ocean, nodes in the atmosphere tend to couple with nodes in the ocean that themselves are mutually connected.

To further quantify the asymmetries in the coupling structure between ocean and atmosphere, we investigate for each node with a given n.s.i. cross-degree density its corresponding n.s.i. local cross-clustering coefficient in a coupled climate network constituted from the SST and (for illustration) the 100 mbar HGT field (Fig. 6). For nodes in the SST field (Fig. 6A) we find that $\mathcal{C}_v^{i*}(\kappa_v^{i*})$ tends to follow a power-law, $\mathcal{C}_v^{i*} \sim (\kappa_v^{i*})^{-1}$, which indicates a hierarchical network structure (Ravasz and Barabási, 2003; Ravasz et al, 2002). Here, hierarchical means that nodes in the SST field couple with disconnected clusters of dynamically similar nodes in the HGT field as depicted in Fig. 5. This deduction is further supported by the fact that for the HGT field, the distribution of combinations of $\mathcal{C}_v^{s*}$ and κ_v^{s*} is more wide-spread and $\mathcal{C}_v^{s*}$ generally takes higher values than $\mathcal{C}_v^{i*}$ implying that nodes in the HGT field show a stronger tendency to connect with connected nodes in the SST field.

The resulting hierarchical network structure may be explained by the presence of large-scale ocean currents, such as the Gulf Stream, the North Atlantic Drift and the North Pacific Current, which cover large fractions of the ocean surface. Each of these areas can be assumed to display a high internal dynamical similarity and, hence, be internally strongly connected in the resulting climate network (Molkenthin et al, 2014; Tupikina et al, 2014). If along the spatial domain covered by each current, the ocean would couple to multiple smaller internally similar areas in the atmosphere, such as those covered by the NAO or the PNA, one would naturally obtain an interaction scheme as illustrated in Fig. 5. To further investigate and test the proposed hypothesis, we plan to study the specific internal structure within the subnetworks in future work.

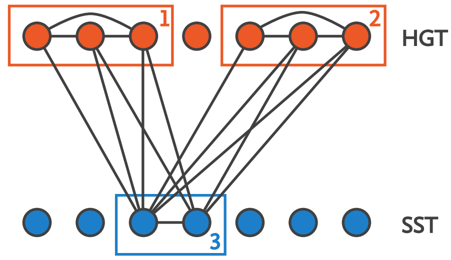

Fig. 5 Schematic explanation of the observed quantitative differences in the n.s.i. local cross-clustering coefficients for nodes in the SST and HGT fields. Nodes in the ocean (box 3) tend to connect with dynamically dissimilar and, hence, unconnected nodes in the atmosphere (such as nodes in box 1 and 2). Hence, the n.s.i. local cross-clustering coefficient $\mathcal{C}_v^{i*}$ only takes low values. In contrast, nodes in the atmosphere, e.g. from box 1, likely connect with mutually connected nodes in the SST field, such as nodes exclusively in box 3. This results in a high n.s.i. cross local-clustering coefficient $\mathcal{C}_v^{s*}$ for nodes in the atmosphere.

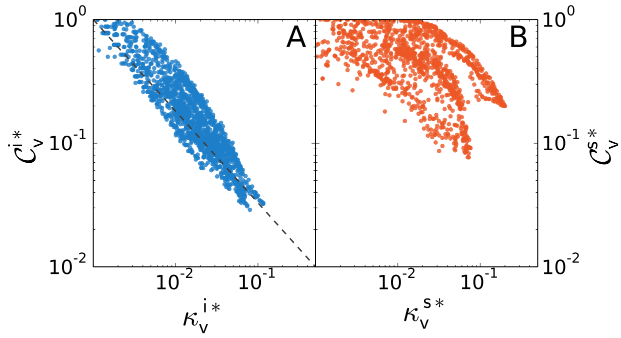

Fig. 6 N.s.i. local cross-clustering coefficients $\mathcal{C}_v^{i*}(\kappa_v^{i*})$ for nodes in the SST field (A) and $\mathcal{C}_v^{s*}(\kappa_v^{s*})$ for nodes in the 100 mbar HGT field (B) as functions of the respective n.s.i. cross-degree densities. The dashed line in (A) indicates the relationship $\mathcal{C}_v^{i*}(\kappa_v^{i*}) \sim (\kappa_v^{i*})^{-1}$ expected for traditional network measures $C_v(k_v)$ in the case of hierarchical network structures (Ravasz and Barabási, 2003; Ravasz et al, 2002).

3.3 Zonally averaged local network measures

To gain further insights into the spatial structure of the ocean-atmosphere interactions, we now examine the coupled climate networks between all 18 HGT fields and the SST field. In order to focus on the main patterns, we first compute zonal averages of the obtained n.s.i. cross-degree density and the n.s.i. local cross-clustering coefficient separately over grid points in the Pacific (from $\phi = 160°$E to $\phi = 140°$W) and the Atlantic (from $\phi = 60°$W to $\phi = 0°$) for all winter months.

The corresponding results are shown in Fig. 7. For the average n.s.i. cross-degree density $\langle\kappa_v^{i*}\rangle_\lambda$ pointing from the SST into the HGT fields, we find constantly high values over the entire range of pressure levels at about $\lambda = 60°$N and between $\lambda = 30°$N and $\lambda = 40°$N in the North Atlantic indicating a strong coupling between the ocean and the troposphere as well as the stratosphere (Fig. 7A). Additionally, maximum values of the average n.s.i. cross-degree density $\langle\kappa_v^{s*}\rangle_\lambda$ pointing from grid points in the HGT networks into the SST network for regions in the Pacific coincide with maxima in observed zonal wind speeds (Fig. 8) averaged over the same time period (DJF) as used in the network construction (Fig. 7B). Up to pressure levels of 100 mbar the average n.s.i. cross-degree density $\langle\kappa_v^{s*}\rangle_\lambda$ takes up its maximum value at around $\lambda = 40°$N, which may be a signature of the subtropical jet stream. For higher levels the maximum is found to shift towards higher latitudes around $\lambda = 80°$N coinciding with the location of the polar vortex (Fig. 8). We note that $\langle\kappa_v^{s*}\rangle_\lambda$ takes lower values above the Atlantic as compared to

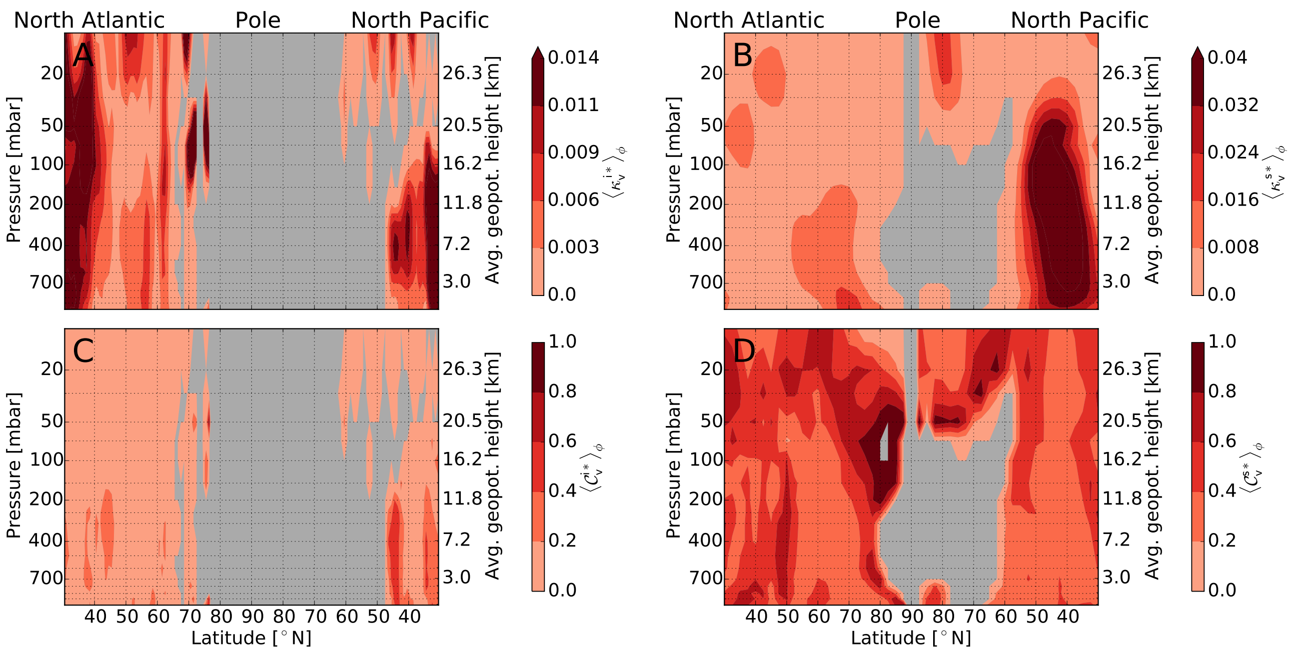

Fig. 7 Zonal averages of n.s.i. cross-degree density $\langle \kappa_v^{i*} \rangle_\lambda$ (A) for nodes in the SST field and $\langle \kappa_v^{s*} \rangle_\lambda$ (B) for nodes in the HGT fields and the n.s.i. local cross-clustering coefficients $\langle \mathcal{C}_v^{i*} \rangle_\lambda$ (C) and $\langle \mathcal{C}_v^{s*} \rangle_\lambda$ (D). For the Pacific, all grid points between $\phi = 160°$E and $\phi = 140°$W and for the Atlantic all grid points between $\phi = 60°$W and $\phi = 0°$ longitude are zonally averaged. Areas with no data or average n.s.i cross-degree density $\langle \kappa_v^{i*} \rangle_\lambda = 0$ and $\langle \kappa_v^{s*} \rangle_\lambda = 0$ are displayed in grey.

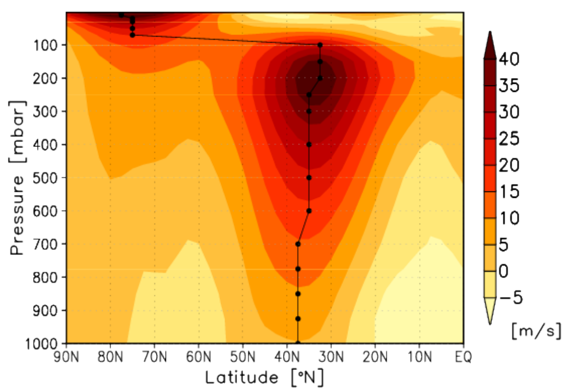

Fig. 8 Average zonal wind speed over the Pacific taken over all grid points between $\phi = 150°$W and $\phi = 120°$E.

the Pacific and, hence, we do not resolve any prominent signatures there. This implies that correlations between both fields generally are higher above the Pacific than above the Atlantic. Choosing a higher cross-link density might overcome this issue. In this case lower correlations would also be considered when constructing the network.

The average local n.s.i. cross-clustering coefficients $\langle \mathcal{C}_v^{i*} \rangle_\lambda$ and $\langle \mathcal{C}_v^{s*} \rangle_\lambda$ estimate the probability for a grid point in one subnetwork to correlate with dynamically similar grid points in the other one (Fig. 7C,D). Analogously to the results presented in Sec. 3.2, we find that grid points in the SST field (Fig. 7C) generally display a low average n.s.i. local cross-clustering coefficient $\langle \mathcal{C}_v^{i*} \rangle_\lambda$ over the whole range of latitudes and layers of geopotential height. Hence, it again seems reasonable to conclude that the ocean-to-atmosphere coupling in the Northern Hemisphere follows a hierarchical structure and nodes in the SST field tend to connect with unconnected nodes in the HGT field. As opposed to this, the average n.s.i. local cross-clustering coefficient $\langle \mathcal{C}_v^{s*} \rangle_\lambda$ for nodes in the HGT field takes also large values over a wide range of latitudes and pressure levels (Fig. 7D) which again hints to a strong localization of coupling between atmospheric layers to the ocean.

We note that particularly the zonally averaged n.s.i. cross-degree density $\langle \kappa_v^{s*} \rangle_\lambda$ for nodes in the different HGT fields (Fig. 7B) is dominated by a strong signal above the North Pacific and, hence, few links are present connecting the SST and HGT fields above the Atlantic. For future research, coupled climate networks could be constructed for the two oceans individually in order to gain information on possible coupling mechanisms above the Atlantic, which display lower correlation and are thus not prominently represented in the present case.

3.4 Global measures

In addition to the local network measures, we also investigate their global counterparts, which characterize the overall topology of the two interacting subnetworks. For each pair of coupled climate networks we investigate the n.s.i. cross-link density, n.s.i. cross-transitivity and n.s.i. global cross-clustering coefficient.

3.4.1 N.s.i. cross-link density

The n.s.i. cross-link density ρ^*_{si} measures the share of mutually connected areas between the two climatological fields with respect to the weight of all possibly connected areas and is displayed in Fig. 9A for different choices of standard cross-link density ρ_{si}. For a fixed cross-link density ρ_{si} it gives a notion of the latitudinal position of areas that are connected with those in the opposite subnetworks, i.e. higher values of ρ^*_{si} indicate for more connections to be present in low latitudes (since the corresponding node weights are higher than those of nodes closer to the pole), whereas low values of ρ^*_{si} indicate a shift of connections towards the poles. We find that for the 400 and 75 mbar pressure levels, ρ^*_{si} takes up its maximum value and displays the lowest values for pressure levels near the Earth's surface and those in the lower stratosphere above 50 mbar which might relate to the presence of the stratospheric polar vortex (Fig. 9A). However, since $\rho^*_{si} = \rho^*_{is}$ is a symmetric measure, it is not visible whether the variation in the n.s.i. cross-link density is preferably induced by latitudinal shifts of strong coupling in the atmosphere or in the ocean.

To further address this issue we additionally compute the area-weighted average cross-degree density

$$\kappa_{si} = \frac{1}{W_i} \sum_{v \in V_s} \kappa^i_v w_v \tag{19}$$

taken over all nodes in the SST and

$$\kappa_{is} = \frac{1}{W_s} \sum_{v \in V_i} \kappa^s_v w_v \tag{20}$$

taken all nodes in the HGT fields individually. This gives an indication of the average latitudinal position of nodes that are likely to couple with those in the opposite subnetwork. As for ρ^*_{si}, a shift of κ_{si} and κ_{is} towards higher values indicates a tendency towards nodes at lower latitudes to display strong interactions with the opposite field.

The area-weighted average cross-degree density κ_{si} for nodes in the SST field is displayed in Fig. 9B and its respective counterpart κ_{is} for nodes in the HGT field in Fig. 9C. We find that the results for ρ^*_{si} and κ_{is} are qualitatively very similar (Fig. 9A,C), whereas we find almost no variation with pressure level for κ_{si} except for the coupling with the lower troposphere (Fig. 9B).

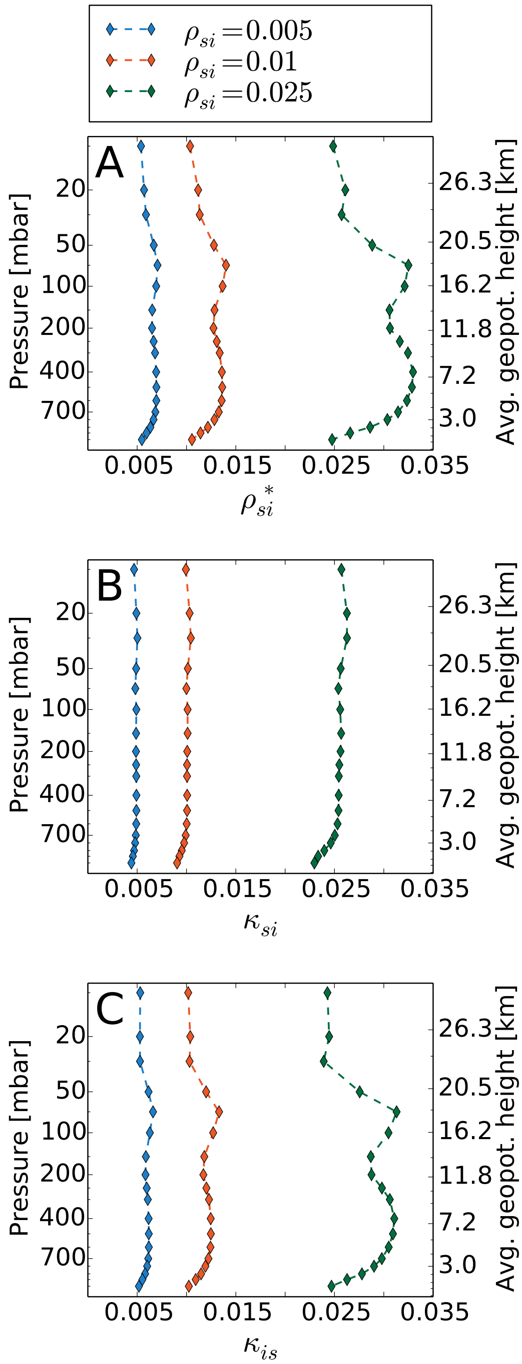

Fig. 9 (A) N.s.i. cross-link density ρ^*_{si} between the SST field and all 18 layers of geopotential height (HGT). Area-weighted average cross-degree densities (B) κ_{si} for nodes in the SST field and (C) κ_{is} for nodes in the HGT fields as defined in Eq. (19) and (20).

Hence, almost no latitudinal dependence of the coupling structure in the ocean is present and we find (on average) that always nodes of the same latitudes in the ocean interact with the atmosphere. This aligns well

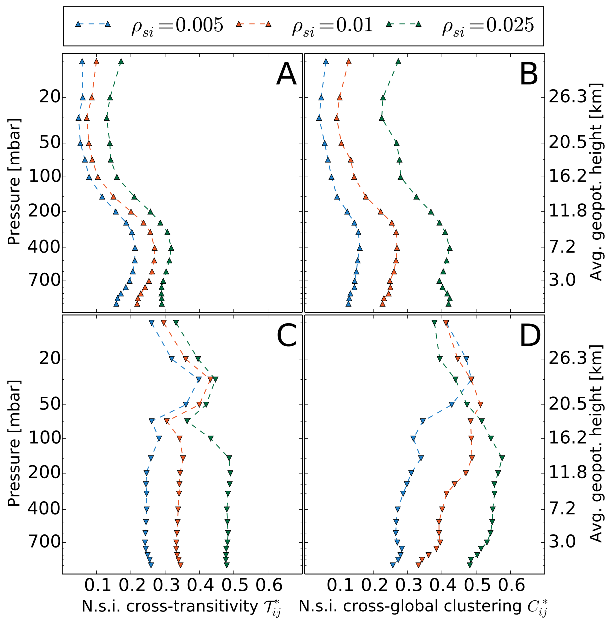

Fig. 10 Global interacting network measures computed for all 18 coupled climate networks. N.s.i. cross-transitivity (A) and n.s.i. global cross-clustering coefficient (B) taken over all nodes in the SST field. (C) and (D) display the respective measures computed over all nodes in the HGT field. To demonstrate the robustness and consistency of the results we construct the networks for different choices of (unweighted) cross-link density ρ_{si} and internal link density $\rho_i = \rho_s = 2\rho_{si}$.

with the hypothesis put forward in Sec. 3.2 regarding a possible role of major ocean currents for the detailed interaction structure and the topology of the resulting climate networks. Since the large-scale flow patterns and, hence, the latitudinal positions of the currents rarely vary with time, the values of κ_{si} are also expected to remain roughly constant (Fig. 9B).

In contrast, the majority of variations in the n.s.i. cross link-density ρ^*_{si} can be related to latitudinal shifts of areas in the atmosphere that interact with the ocean. We find the same distinct maxima in κ_{is} for the 400 and 75 mbar HGT fields that were present for ρ^*_{si} (Fig. 9A,C). Thus, for these pressure levels interactions preferably take place between the ocean and parts of the atmosphere further towards the equator as compared to other layers of HGT.

3.4.2 N.s.i. cross-transitivity and n.s.i. global cross-clustering coefficient

Finally, we investigate the n.s.i. cross-transitivity $\mathcal{T}^*_{si}$ computed over nodes in the SST field and $\mathcal{T}^*_{is}$ computed over nodes in each of the HGT fields according to Eq. (18) together with the n.s.i. global cross-clustering coefficients $\mathcal{C}^*_{si}$ and $\mathcal{C}^*_{is}$, respectively (Eq. (16)), Fig. 10. Both $\mathcal{T}^*_{si}$ and $\mathcal{C}^*_{si}$ show their maximum values at around 10 km (250 mbar), which coincides with the maximum of the jet wind speed in winter (Figs. 10A and 10B). For the same quantities, distinct minima at 850 mbar (1.4 km) coincide with the transition from the atmospheric boundary layer to the lower troposphere (as in Donges et al, 2011). For all layers above 100 mbar particularly $\mathcal{T}^*_{si}$ remains almost constant at low values. Hence, $\mathcal{T}^*_{si}$ and $\mathcal{C}^*_{si}$ seem to naturally discriminate the atmosphere into three different layers: Those below 850 mbar (the atmospheric boundary layer), those between 850 mbar and 100 mbar (the free atmosphere) and those above 100 mbar (the lower stratosphere).

For the global measures computed over all nodes in the HGT field, we find that the n.s.i. cross-transitivity $\mathcal{T}^*_{is}$ shows almost constant values for all layers below 200 mbar and, hence, again separates well the dynamics within the troposphere from that inside the stratosphere, Fig. 10C. For all layers above 200 mbar $\mathcal{T}^*_{is}$ becomes almost independent of the cross-link density ρ_{si} that is fixed when constructing the network. The same property holds also for the n.s.i. global cross-clustering coefficient $\mathcal{C}^*_{is}$ computed over all nodes in the HGT field, Fig. 10D.

In agreement with the (averaged) local measures discussed in Sec. 3.2 and 3.3 we find that the n.s.i. cross-transitivity and n.s.i. global cross-clustering coefficients are larger for nodes in the HGT fields than for nodes in the SST field (compare Fig. 10A with Fig. 10C and Fig. 10B with Fig. 10D). As for the n.s.i. local cross-clustering coefficients this indicates again the hierarchical network structure, e.g., a higher tendency for nodes in the HGT field to form triangular structures with nodes in the SST field, that is present across all atmospheric layers. The detailed structure of this hierarchical coupling, however, seems to vary with the different atmospheric layers under study.

In general, we observe that the quantitative and qualitative properties of the n.s.i. cross-transitivity and n.s.i. global cross-clustering coefficients vary with the different atmospheric layers. Hence, these global characteristics may serve as a quantifier to inter-compare and distinguish between different types of coupling structures in a coupled climate network. An in-depth analysis of the mechanisms that cause the occurrence of this behavior in our specific application remains as a subject of future research.

4 Conclusions

We have carried out a detailed analysis of the interaction structure between atmospheric and ocean dynamics in the Northern Hemisphere from the viewpoint of coupled climate networks. Comparison between the n.s.i. cross-degree density (measuring the weighted share of significant correlations between grid points in different layers) and the leading mode of the maximum covariance analysis (MCA) reveals an expected high congruence between both methods for the considered data sets. However, network analysis, and particularly the investigation of higher-order network parameters, allows us to further disentangle the underlying interaction structure. The (average) n.s.i. cross-degree density in combination with the (average) n.s.i. local cross-clustering coefficient provides insights on areas in the ocean and the atmosphere that show significant coupling as well as localized versus delocalized interaction structures with the respective opposite field. In the SST field nodes tend to couple with multiple unconnected clusters of dynamically similar nodes within the respective HGT fields. From investigating the interdependency between n.s.i. cross-degree density and n.s.i. local cross-clustering coefficient, we found that the coupling from the ocean to the atmosphere follows a hierarchical structure, which might be related to large-scale ocean currents that couple with different dynamically dissimilar areas along their respective direction of flow.

Additionally, our analysis recaptures dominant signatures such as jet stream patterns and the polar vortex. Global network characteristics further support the results obtained from their local correspondents and provide insights into the overall interaction structure between ocean and atmosphere. Hence, complex network theory serves as a powerful tool for addressing these issues complementing other well-established methods from statistical climatology.

Future work should also study the internal network structure within each of the climatological fields in order to further investigate the processes that cause the presence of the observed hierarchical interacting network structure. To this end, our analysis has only been performed for the pairwise coupling between one atmospheric layer and the ocean. Thus, future studies should investigate the possibility to refine the proposed methods to also quantify interactions in a climate network that decomposes into more than two subnetworks. Specifically, when studying coupled climate networks in the Northern hemisphere one should also consider Arctic sea ice concentration as an additional observable in the network construction. Its dynamics have already been discovered as an influencing factor on atmospheric teleconnections and the dynamics of land snow cover in the Northern hemisphere (Handorf et al, 2015). The study of coupled climate networks can help here to further disentangle and quantify possible changes in interactions between ocean and atmosphere over the course of the past decades that may be induced by processes related to the Arctic amplification (Serreze and Francis, 2006). Moreover, it is of great interest to apply these methods not only to an interacting network composed of different climatological fields, but also to a network constructed from a single field that divides into dynamically distinct areas, usually denoted as communities (Tsonis et al, 2010; Steinhaeuser et al, 2011). This would allow for a detailed investigation of correlation structures between different climatic subsystems such as, for example, the Indian Summer Monsoon and the El Niño Southern Oscillation (Hlinka et al, 2014).

Finally, it remains to remark that the weighted network measures presented in this work provide a general framework which can be applied to quantify interdependencies in complex networks representing subjects of study taken from many other fields beyond climatology.

Acknowledgements MW and RVD have been supported by the German Federal Ministry for Education and Research via the BMBF Young Investigators Group CoSy-CC^2 (grant no. 01LN1306A). JFD thanks the Stordalen Foundation and BMBF (project GLUES) for financial support. JK acknowledges the IRTG 1740 funded by DFG and FAPESP. Coupled climate network analysis has been performed using the Python package `pyunicorn` (Donges et al, 2013) that is available at `https://github.com/pik-copan/pyunicorn`.

References

Albert R, Barabási AL (2002) Statistical mechanics of complex networks. Rev Mod Phys 74(1):47–97

An SI, Wang B (2005) The Forced and Intrinsic Low-Frequency Modes in the North Pacific. J Climate 18(6):876–885, DOI 10.1175/JCLI-3298.1

Boccaletti S, Bianconi G, Criado R, del Genio CI, Gómez-Gardeñes J, Romance M, Sendiña-Nadal I, Wang Z, Zanin M (2014) The structure and dynamics of multilayer networks. Physics Reports 544(1):1–122, DOI 10.1016/j.physrep.2014.07.001

Boers N, Bookhagen B, Marwan N, Kurths J, Marengo J (2013) Complex networks identify spatial patterns of extreme rainfall events of the South American Monsoon System. Geophys Res Lett 40(16):4386–4392, DOI 10.1002/grl.50681

Boers N, Bookhagen B, Barbosa HMJ, Marwan N, Kurths J, Marengo JA (2014a) Prediction of extreme floods in the eastern Central Andes based on a complex networks approach. Nat Commun 5(5199), DOI 10.1038/ncomms6199

Boers N, Donner RV, Bookhagen B, Kurths J (2014b) Complex network analysis helps to identify impacts of the El Niño Southern Oscillation on moisture divergence in South America. Clim Dyn DOI 10.1007/s00382-014-2265-7

Bretherton CS, Smith C, Wallace JM (1992) An Intercomparison of Methods for Finding Coupled Patterns in Climate Data. J Climate 5(6):541–560, DOI 10.1175/1520-0442(1992)005⟨0541:AIOMFF⟩2.0.CO;2

Buldyrev SV, Parshani R, Paul G, Stanley HE, Havlin S (2010) Catastrophic cascade of failures in interdependent networks. Nature 464(7291):1025–1028, DOI 10.1038/nature08932

Czaja A, Frankignoul C (1999) Influence of the North Atlantic SST on the atmospheric circulation. Geophys Res Lett 26(19):2969–2972, DOI 10.1029/1999GL900613

Czaja A, Frankignoul C (2002) Observed Impact of Atlantic SST Anomalies on the North Atlantic Oscillation. J Climate 15(6):606–623, DOI 10.1175/1520-0442(2002)015⟨0606:OIOASA⟩2.0.CO;2

Donges JF, Zou Y, Marwan N, Kurths J (2009a) The backbone of the climate network. Europhys Lett 87(4):48,007, DOI 10.1209/0295-5075/87/48007

Donges JF, Zou Y, Marwan N, Kurths J (2009b) Complex networks in climate dynamics. Eur Phys J Spec Top 174(1):157–179, DOI 10.1140/epjst/e2009-01098-2

Donges JF, Schultz HCH, Marwan N, Zou Y, Kurths J (2011) Investigating the topology of interacting networks. Eur Phys J B 84(4):635–651, DOI 10.1140/epjb/e2011-10795-8

Donges JF, Heitzig J, Donner RV, Kurths J (2012) Analytical framework for recurrence network analysis of time series. Phys Rev E 85(4):046–105, DOI 10.1103/PhysRevE.85.046105

Donges JF, Heitzig J, Runge J, Schultz HCH, Wiedermann M, Zech A, Feldhoff J, Rheinwalt A, Kutza H, Radebach A, Marwan N, Kurths J (2013) Advanced functional network analysis in the geosciences: The pyunicorn package. In: EGU General Assembly Conference Abstracts, vol 15, p 3558

Donges JF, Petrova I, Loew A, Marwan N, Kurths J (2015) How complex climate networks complement eigen techniques for the statistical analysis of climatological data. Clim Dyn DOI 10.1007/s00382-015-2479-3

Donner RV, Zou Y, Donges JF, Marwan N, Kurths J (2010) Recurrence networks—a novel paradigm for nonlinear time series analysis. New J Phys 12(3):033,025, DOI 10.1088/1367-2630/12/3/033025

Feng A, Gong Z, Wang Q, Feng G (2012) Three-dimensional air–sea interactions investigated with bilayer networks. Theor Appl Climatol 109(3-4):635–643, DOI 10.1007/s00704-012-0600-7

Feng QY, Dijkstra H (2014) Are North Atlantic multidecadal SST anomalies westward propagating? Geophys Res Lett 41(2):541–546, DOI 10.1002/2013GL058687

Feng QY, Viebahn JP, Dijkstra HA (2014) Deep ocean early warning signals of an Atlantic MOC collapse. Geophys Res Lett 41(16):6009–6015, DOI 10.1002/2014GL061019

Frankignoul C, Sennchael N (2007) Observed Influence of North Pacific SST Anomalies on the Atmospheric Circulation. J Climate 20(3):592–606, DOI 10.1175/JCLI4021.1

Frankignoul C, de Coëtlogon G, Joyce TM, Dong S (2001) Gulf Stream Variability and Ocean–Atmosphere Interactions. J Phys Oceanogr 31(12):3516–3529, DOI 10.1175/1520-0485(2002)031⟨3516:GSVAOA⟩2.0.CO;2

Gastineau G, Frankignoul C (2014) Influence of the North Atlantic SST Variability on the Atmospheric Circulation during the Twentieth Century. J Climate 28(4):1396–1416, DOI 10.1175/JCLI-D-14-00424.1

Ghil M, Allen MR, Dettinger MD, Ide K, Kondrashov D, Mann ME, Robertson AW, Saunders A, Tian Y, Varadi F, Yiou P (2002) Advanced Spectral Methods for Climatic Time Series. Rev Geophys 40(1):1003, DOI 10.1029/2000RG000092

Handorf D, Jaiser R, Dethloff K, Rinke A, Cohen J (2015) Impacts of Arctic sea ice and continental snow cover changes on atmospheric winter teleconnections. Geophys Res Lett 42(7):2367–2377, DOI 10.1002/2015GL063203

Hannachi A, Jolliffe IT, Stephenson DB (2007) Empirical orthogonal functions and related techniques in atmospheric science: A review. Int J Climatol 27(9):1119–1152, DOI 10.1002/joc.1499

Heitzig J, Donges JF, Zou Y, Marwan N, Kurths J (2012) Node-weighted measures for complex networks with spatially embedded, sampled, or differently sized nodes. Eur Phys J B 85(1):38, DOI 10.1140/epjb/e2011-20678-7

Hlinka J, Hartman D, Jajcay N, Vejmelka M, Donner R, Marwan N, Kurths J, Paluš M (2014) Regional and inter-regional effects in evolving climate networks. Nonlin Processes Geophys 21(2):451–462, DOI 10.5194/npg-21-451-2014

Kwon YO, Alexander MA, Bond NA, Frankignoul C, Nakamura H, Qiu B, Thompson LA (2010) Role of the Gulf Stream and Kuroshio-Oyashio systems in large-scale atmosphere-ocean interaction: A review. J Climate 23(12):3249–3281, DOI 10.1175/2010JCLI3343.1

Liu Q, Wen N, Liu Z (2006) An observational study of the impact of the North Pacific SST on the atmosphere. Geophys Res Lett 33(18):L18,611, DOI 10.1029/2006GL026082

Ludescher J, Gozolchiani A, Bogachev MI, Bunde A, Havlin S, Schellnhuber HJ (2013) Improved El Niño forecasting by cooperativity detection. PNAS 110(29):11,742–11,745, DOI 10.1073/pnas.1309353110

Ludescher J, Gozolchiani A, Bogachev MI, Bunde A, Havlin S, Schellnhuber HJ (2014) Very early warning of next El Niño. PNAS 111(6):2064–2066, DOI 10.1073/pnas.1323058111

Malik N, Marwan N, Kurths J (2010) Spatial structures and directionalities in Monsoonal precipitation over South Asia. Nonlin Processes Geophys 17(5):371–381, DOI 10.5194/npg-17-371-2010

Malik N, Bookhagen B, Marwan N, Kurths J (2011) Analysis of spatial and temporal extreme monsoonal rainfall over South Asia using complex networks. Clim Dyn 39(3-4):971–987, DOI 10.1007/s00382-011-1156-4

van der Mheen M, Dijkstra HA, Gozolchiani A, den Toom M, Feng Q, Kurths J, Hernandez-Garcia E (2013) Interaction network based early warning indicators for the Atlantic MOC collapse. Geophys Res Lett 40(11):2714–2719, DOI 10.1002/grl.50515

Molkenthin N, Rehfeld K, Marwan N, Kurths J (2014) Networks from Flows - From Dynamics to Topology. Sci Rep 4(4119), DOI 10.1038/srep04119

Newman M (2003) The Structure and Function of Complex Networks. SIAM Rev 45(2):167–256, DOI 10.1137/S003614450342480

Nonaka M, Xie SP (2003) Covariations of Sea Surface Temperature and Wind over the Kuroshio and its extension: Evidence for Ocean-to-Atmosphere feedback. J Climate 16(9):1404–1413, DOI 10.1175/1520-0442(2003)16⟨1404:COSSTA⟩2.0.CO;2

Paluš M, Hartman D, Hlinka J, Vejmelka M (2011) Discerning connectivity from dynamics in climate networks. Nonlin Processes Geophys 18(5):751–763, DOI 10.5194/npg-18-751-2011

Radebach A, Donner RV, Runge J, Donges JF, Kurths J (2013) Disentangling different types of El Niño episodes by evolving climate network analysis. Phys Rev E 88(5):052–807, DOI 10.1103/PhysRevE.88.052807

Ravasz E, Barabási AL (2003) Hierarchical organization in complex networks. Phys Rev E 67(2):026–112, DOI 10.1103/PhysRevE.67.026112

Ravasz E, Somera AL, Mongru DA, Oltvai ZN, Barabási AL (2002) Hierarchical Organization of Modularity in Metabolic Networks. Science 297(5586):1551–1555, DOI 10.1126/science.1073374

Rayner NA, Parker DE, Horton EB, Folland CK, Alexander LV, Rowell DP, Kent EC, Kaplan A (2003) Global analyses of sea surface temperature, sea ice, and night marine air temperature since the late nineteenth century. J Geophys Res 108(D14):4407, DOI 10.1029/2002JD002670

Serreze MC, Francis JA (2006) The Arctic Amplification Debate. Climatic Change 76(3-4):241–264, DOI 10.1007/s10584-005-9017-y

Steinhaeuser K, Ganguly AR, Chawla NV (2011) Multivariate and multiscale dependence in the global climate system revealed through complex networks. Clim Dyn 39(3-4):889–895, DOI 10.1007/s00382-011-1135-9

Stolbova V, Martin P, Bookhagen B, Marwan N, Kurths J (2014) Topology and seasonal evolution of the network of extreme precipitation over the Indian subcontinent and Sri Lanka. Nonlin Processes Geophys 21(4):901–917, DOI 10.5194/npg-21-901-2014

von Storch H, Zwiers FW (2001) Statistical Analysis in Climate Research. Cambridge University Press

Tantet A, Dijkstra HA (2014) An interaction network perspective on the relation between patterns of sea surface temperature variability and global mean surface temperature. Earth Syst Dynam 5(1):1–14, DOI 10.5194/esd-5-1-2014

Trenberth KE, Hurrell JW (1994) Decadal atmosphere-ocean variations in the Pacific. Climate Dynamics 9(6):303–319, DOI 10.1007/BF00204745

Tsonis AA, Roebber PJ (2004) The architecture of the climate network. Physica A 333:497–504, DOI 10.1016/j.physa.2003.10.045

Tsonis AA, Swanson KL, Roebber PJ (2006) What Do Networks Have to Do with Climate? Bull Amer Meteor Soc 87(5):585–595, DOI 10.1175/BAMS-87-5-585

Tsonis AA, Swanson KL, Wang G (2008) On the Role of Atmospheric Teleconnections in Climate. J Climate 21(12):2990–3001, DOI 10.1175/2007JCLI1907.1

Tsonis AA, Wang G, Swanson KL, Rodrigues FA, Costa LdF (2010) Community structure and dynamics in climate networks. Clim Dyn 37(5-6):933–940, DOI 10.1007/s00382-010-0874-3

Tupikina L, Rehfeld K, Molkenthin N, Stolbova V, Marwan N, Kurths J (2014) Characterizing the evolution of climate networks. Nonlin Processes Geophys 21(3):705–711, DOI 10.5194/npg-21-705-2014

Uppala SM, Kållberg PW, Simmons AJ, Andrae U, Bechtold VDC, Fiorino M, Gibson JK, Haseler J, Hernandez A, Kelly GA, Li X, Onogi K, Saarinen S, Sokka N, Allan RP, Andersson E, Arpe K, Balmaseda MA, Beljaars ACM, Berg LVD, Bidlot J, Bormann N, Caires S, Chevallier F, Dethof A, Dragosavac M, Fisher M, Fuentes M, Hagemann S, Hólm E, Hoskins BJ, Isaksen L, Janssen PaEM, Jenne R, Mcnally AP, Mahfouf JF, Morcrette JJ, Rayner NA, Saunders RW, Simon P, Sterl A, Trenberth KE, Untch A, Vasiljevic D, Viterbo P, Woollen J (2005) The ERA-40 re-analysis. Q J Roy Meteor Soc 131(612):2961–3012, DOI 10.1256/qj.04.176

Vespignani A (2010) Complex networks: The fragility of interdependency. Nature 464(7291):984–985, DOI 10.1038/464984a

Wallace JM, Zhang Y, Bajuk L (1996) Interpretation of interdecadal trends in northern hemisphere surface air temperature 9(2):249–259, DOI 10.1175/1520-0442(1996)009⟨0249:IOITIN⟩2.0.CO;2

Wen N, Liu Z, Liu Q, Frankignoul C (2005) Observations of SST, heat flux and North Atlantic Ocean-atmosphere interaction. Geophys Res Lett 32(24):L24,619, DOI 10.1029/2005GL024871

Wiedermann M, Donges JF, Heitzig J, Kurths J (2013) Node-weighted interacting network measures improve the representation of real-world complex systems. Europhys Lett 102(2):28,007, DOI 10.1209/0295-5075/102/28007

Woollings T, Hannachi A, Hoskins B (2010) Variability of the North Atlantic eddy-driven jet stream. Q J Roy Meteor Soc 136(649):856–868, DOI 10.1002/qj.625

Wyrtki K (1975) El Niño – The Dynamic Response of the Equatorial Pacific Oceanto Atmospheric Forcing. J Phys Oceanogr 5(4):572–584, DOI 10.1175/1520-0485(1975)005⟨0572:ENTDRO⟩2.0.CO;2

Zemp DC, Wiedermann M, Kurths J, Rammig A, Donges JF (2014) Node-weighted measures for complex networks with directed and weighted edges for studying continental moisture recycling. Europhys Lett 107(5):58,005, DOI 10.1209/0295-5075/107/58005

A Similarities between leading coupled patterns and n.s.i. cross-degree densities

Following Donges et al (2015), we derive relationships between degree-related weighted and unweighted measures for coupled climate networks and the corresponding coupled patterns from weighted MCA. In this work, coupled patterns $\mathbf{p}_s^{(k)}$ and $\mathbf{p}_i^{(k)}$ (see Eqs. (3)-(4)) are computed from the weighted cross-correlation matrix (Eq. 2) between two climatological fields with elements

$$\begin{aligned} C^w_{s_n i_m} &= w_{s_n i_m} C_{s_n i_m} \\ &= \sqrt{\cos\lambda_{s_n}\cos\lambda_{i_m}}\, C_{s_n i_m} \end{aligned} \tag{21}$$

with $w_{s_n i_m} = \sqrt{\cos\lambda_{s_n}\cos\lambda_{i_m}}$ according to Eq. (2). The weighted cross-covariance matrix can be expanded in terms of coupled patterns and singular values as

$$C^w_{s_n i_m} = \sum_{k=1}^{R} \sigma_k p^{(k)}_{s_n} p^{(k)}_{i_m}. \tag{22}$$

This implies that the unweighted cross-correlation matrix can be expressed as

$$C_{s_n i_m} = \frac{1}{w_{s_n i_m}} \sum_{k=1}^{R} \sigma_k p^{(k)}_{s_n} p^{(k)}_{i_m}. \tag{23}$$

Since all coupled climate network measures are based on $C_{s_n i_m}$, degree-based measures can be written as functions of singular values and coupled patterns from weighted MCA as well. For the unweighted cross-degree, we obtain

$$\begin{aligned} k^s_m &= \sum_{n=1}^{N_s} \Theta\left(|C_{s_n i_m}| - T_{si}\right) \\ &= \sum_{n=1}^{N_s} \Theta\left(\frac{1}{w_{s_n i_m}}\left|\sum_{k=1}^{R}\sigma_k p^{(k)}_{s_n} p^{(k)}_{i_m}\right| - T_{si}\right) \end{aligned} \tag{24}$$

and analogously

$$\begin{aligned} k^i_n &= \sum_{m=1}^{N_i} \Theta\left(|C_{s_n i_m}| - T_{si}\right) \\ &= \sum_{m=1}^{N_i} \Theta\left(\frac{1}{w_{s_n i_m}}\left|\sum_{k=1}^{R}\sigma_k p^{(k)}_{s_n} p^{(k)}_{i_m}\right| - T_{si}\right). \end{aligned} \tag{25}$$

Similarly, for the n.s.i. cross-degree one obtains

$$\begin{aligned} k^{s*}_m &= \sum_{n=1}^{N_s} w_n \Theta\left(|C_{s_n i_m}| - T_{si}\right) \\ &= \sum_{n=1}^{N_s} w_n \Theta\left(\frac{1}{w_{s_n i_m}}\left|\sum_{k=1}^{R}\sigma_k p^{(k)}_{s_n} p^{(k)}_{i_m}\right| - T_{si}\right) \end{aligned} \tag{26}$$

and

$$\begin{aligned} k^{i*}_n &= \sum_{m=1}^{N_i} w_m \Theta\left(|C_{s_n i_m}| - T_{si}\right) \\ &= \sum_{m=1}^{N_i} w_m \Theta\left(\frac{1}{w_{s_n i_m}}\left|\sum_{k=1}^{R}\sigma_k p^{(k)}_{s_n} p^{(k)}_{i_m}\right| - T_{si}\right). \end{aligned} \tag{27}$$

Analogous results hold for the cross-degree and n.s.i. cross-degree densities, respectively.

In the following, we focus on the n.s.i. cross-degree k^{s*}_m for illustration, while all results hold for the other degree-related measures as well. If the leading pair of coupled patterns explains a large fraction of the cross-covariance between both climatological fields with $\sigma_1 \gg \sigma_2$ (as is the case for the climatological fields investigated in this study), we can approximate

$$k^{s*}_m \approx \sum_{n=1}^{N_s} w_n \Theta\left(\frac{\sigma_1}{w_{s_n i_m}}\left|p^{(1)}_{s_n} p^{(1)}_{i_m}\right| - T_{si}\right) \tag{28}$$

Elements of the leading coupled pattern $p^{(1)}_{i_m}$ contribute to this sum if $|p^{(1)}_{i_m}| \geq T_{si} w_{s_n i_m}/\sigma_1 |p^{(1)}_{s_n}|$. Hence, a larger $|p^{(1)}_{i_m}|$ increases the odds for a larger k^{s*}_m to arise, implying a positive correlation between the absolute coefficient of the leading coupled pattern $|p^{(1)}_{i_m}|$ and the n.s.i. cross-degree k^{s*}_m as well as the n.s.i. cross-degree density $\kappa^{s*}_m = k^{s*}_m / W_s$, as it is observed in this study (Section 3.2).